Molecular Therapy
Nucleic Acids
Original Article

MicroRNA-451a inhibits gemcitabine-refractory biliary tract cancer progression by suppressing the MIF-mediated PI3K/AKT pathway

Taisuke Obata,[1] Koichiro Tsutsumi,[2] Eijiro Ueta,[2] Takashi Oda,[1] Tatsuya Kikuchi,[1] Soichiro Ako,[2] Yuki Fujii,[2] Tatsuhiro Yamazaki,[2] Daisuke Uchida,[2] Kazuyuki Matsumoto,[2] Shigeru Horiguchi,[2] Hironari Kato,[2] Hiroyuki Okada,[1,2] and Motoyuki Otsuka[1,2]

[1]Department of Gastroenterology and Hepatology, Okayama University Graduate School of Medicine, Dentistry, and Pharmaceutical Science, Okayama 700-8558, Japan; [2]Department of Gastroenterology and Hepatology, Okayama University Hospital, Okayama 700-8558, Japan

Gemcitabine is an effective chemotherapeutic agent for biliary tract cancers (BTCs), including gallbladder cancer (GBC) and cholangiocarcinoma (CCA). However, few other effective agents are currently available, particularly for GEM-refractory BTCs. We previously identified microRNA-451a (miR-451a) as a potential therapeutic target in GBC. To elucidate the antineoplastic effects of miR-451a and its underlying mechanisms, we transfected miR-451a into GBC, gemcitabine-resistant GBC (GR-GBC), and gemcitabine-resistant CCA (GR-CCA) cell lines. Furthermore, mimicking *in vivo* conditions, tumorigenic GBC organoids and three-dimensional (3D) cell culture systems were employed to investigate the anti-proliferative effects of miR-451a on BTCs, and its effect on stem cell properties. We found that miR-451a significantly inhibited cell proliferation, induced apoptosis, and reduced chemoresistant phenotypes, such as epithelial-mesenchymal transition, in both GBC and GR-GBC. The principal mechanism is probably the negative regulation of the phosphatidylinositol 3-kinase/AKT pathway, partially accomplished by directly downregulating macrophage migration inhibitory factor. The Gene Expression Omnibus database revealed that miR-451a was the most significantly downregulated microRNA in CCA tissues. The introduction of miR-451a resulted in similar antineoplastic effects in GR-CCA. Furthermore, miR-451a reduced cell viability in 3D spheroid models and tumorigenic GBC organoids. These findings suggest that the supplementation of miR-451a is a potential treatment strategy for GEM-refractory BTCs.

INTRODUCTION

Biliary tract cancers (BTCs), including intrahepatic and extrahepatic cholangiocarcinoma (CCA) and gallbladder cancer (GBC), are highly prevalent in Asia and South America. In addition, the incidence of BTC is increasing globally.[1–3] Surgery is currently the best curative treatment for BTCs; however, most patients are diagnosed with locally advanced and metastatic BTC because of the lack of symptoms.[4,5] Furthermore, the decision of treatment regimens is sometimes difficult, even for small BTCs, because of the complexity of the hepatobiliary-pancreatic system.[6] The current standard chemotherapy is the combination of gemcitabine (GEM) and cisplatin for advanced-stage BTCs,[7] and recently, anti-programmed death cell ligand 1 durvalumab is also used in combination with GEM and cisplatin.[8] Other combinations, including 5-fluorouracil, oxaliplatin, and capecitabine, are also recommended.[9] Also, novel molecular targeted drugs have been developed for specific genetic mutations, including pembrolizumab for high microsatellite instability, pemigatinib or infigratinib for *FGFR2* fusions or rearrangements, entrectinib or larotrectinib for *NTRK* gene fusion, and ivosidenib for *IDH1* mutations.[1] However, these drugs can be used in only a few BTC cases (<10%).[10] Therefore, developing new therapeutic agents for BTCs is urgently needed, particularly for patients with GEM-refractory BTCs.

Nucleic acid-based therapies involving microRNAs (miRNAs) are promising cancer treatment strategies.[11] miRNAs are small non-coding RNA molecules that regulate gene expression post-transcriptionally; approximately 2,700 mature human miRNAs have been identified.[12–16] Dysregulated miRNAs contribute to cancer pathogenesis.[13,14] Therefore, miRNA profiling has been used to identify signatures associated with cancer diagnosis, progression, prognosis, and treatment response.[15] Moreover, clinical trials of miRNA replacement therapies are ongoing, continuously demonstrating the potential of this approach for cancer treatment.[17,18] However, little is known about the miRNA targets that can overcome BTCs, especially those with acquired resistance to GEM.

Received 1 June 2023; accepted 11 October 2023; Published: October 27, 2023.
https://doi.org/10.1016/j.omtn.2023.102054.

Correspondence: Koichiro Tsutsumi, MD, PhD, Department of Gastroenterology and Hepatology, Okayama University Hospital, 2-5-1 Shikata-cho, Kita-ku, Okayama-city, Okayama 700-8558, Japan.
E-mail: tsutsumi@okayama-u.ac.jp
Correspondence: Motoyuki Otsuka, MD, PhD, Department of Gastroenterology and Hepatology, Okayama University Hospital, 2-5-1 Shikata-cho, Kita-ku, Okayama-city, Okayama 700-8558, Japan.
E-mail: otsukamoto@okayama-u.ac.jp

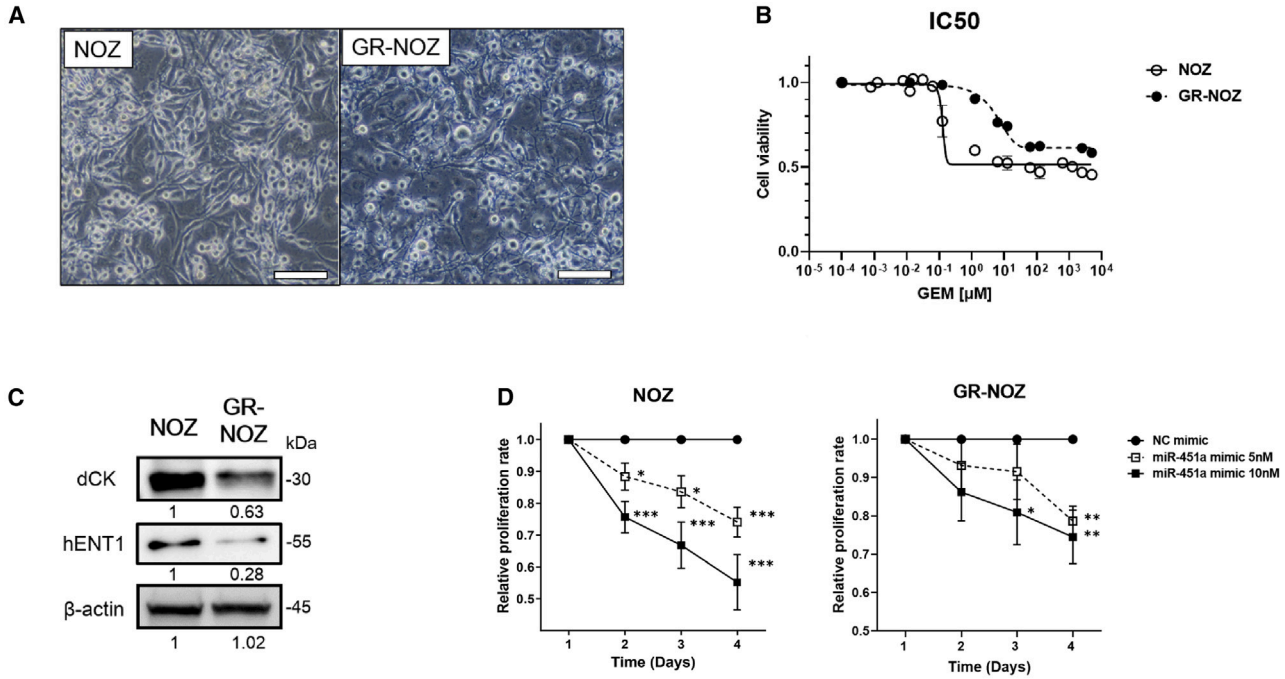

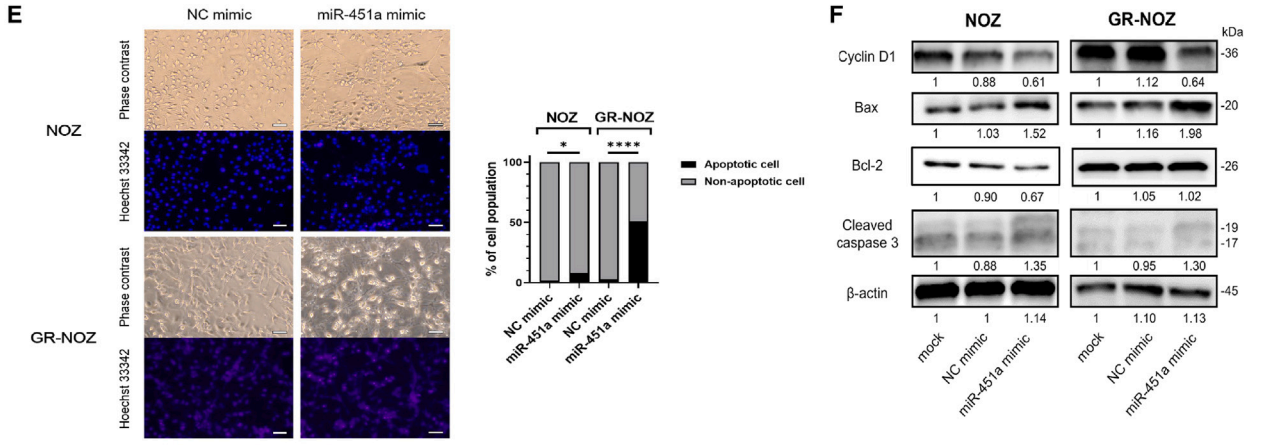

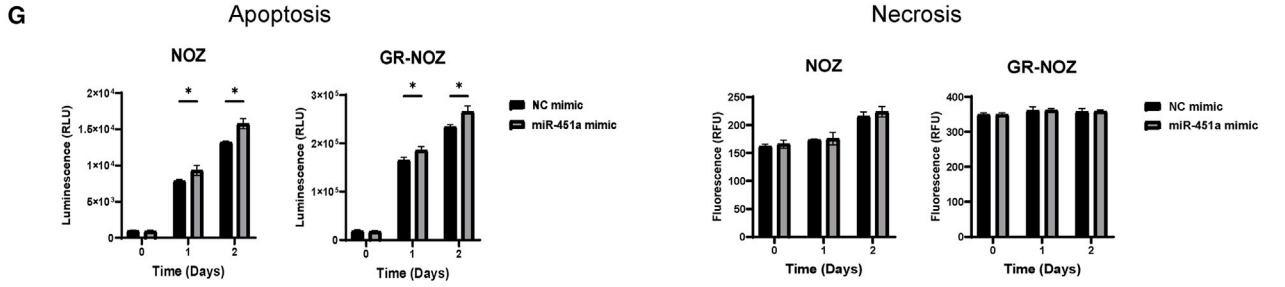

(legend on next page)

In our previous study, we investigated serum markers for diagnosing and predicting the prognosis of GBC,[19] focusing on miRNAs in small extracellular vesicles (EVs) protected by a lipid bilayer membrane.[20] In the miRNA expression analysis of 119 serum EV samples from patients with GBC, benign gallbladder diseases, and healthy controls, we found that microRNA-451a (miR-451a) was significantly downregulated in the serum EVs and tissues of patients with GBC compared with those without GBC.[19] Moreover, transfection of an miR-451a mimic into human GBC cell lines inhibited cell proliferation. Several studies reported the aberrant expression of miR-451a and its association with the clinical outcomes in various types of cancers,[21] including lung cancer,[22] hepatocellular carcinoma,[23] and renal cell carcinoma.[24] These data suggest that miR-451a may also be a therapeutic target against GBC. However, the mechanism through which miR-451a suppresses GBC cell growth remains unclear. Its efficacy against GEM-resistant GBC (GR-GBC) and the possible application of miR-451a in GEM-resistant CCA (GR-CCA) remains to be investigated.

This study investigated the antineoplastic effects and mechanism of action of miR-451a in GBC cells. In addition, to further elucidate the potential of miR-451a replacement therapy for treating GEM-refractory BTC, we evaluated the effectiveness of miR-451a against GR-GBC and GR-CCA using two-dimensional (2D) and three-dimensional (3D) cell culture systems.

RESULTS

miR-451a inhibits cell proliferation and induces apoptosis in NOZ and GR-NOZ cells

The established GEM-resistant NOZ (GR-NOZ) cells were characterized and compared with NOZ cells. Both the cell lines were mostly spindle-shaped (Figure 1A). However, the half-maximal inhibitory concentration (IC50) of GEM was 10 μM in NOZ cells and >5 mM in GR-NOZ cells (Figure 1B), confirming that GR-NOZ cells acquired GEM resistance. Furthermore, per the alteration of GEM sensitivity, the expression of two GEM-related proteins, human equilibrative nucleoside transporter1 (hENT1) and deoxycytidine kinase (dCK), decreased in GR-NOZ cells (Figure 1C). For subsequent experiments in the 2D and 3D cell culture systems, these two cell lines were used as GBC cell lines with or without GEM resistance.

First, cell proliferation was significantly inhibited in a dose-dependent manner in NOZ cells transfected with the miR-451a mimic compared with cells transfected with the negative control (NC) mimic ($p < 0.005$; Figure 1D). Similarly, cell growth was significantly inhibited in GR-NOZ cells after transfection with the miR-451a mimic ($p < 0.01$). Furthermore, microscopic examination revealed floating, round, or chromatin-concentrated cells, and Hoechst staining demonstrated significantly more cells with nuclear condensation after transfection with the miR-451a mimic than after transfection with the NC mimic (NOZ, $p < 0.05$; GR-NOZ, $p < 0.001$; Figure 1E), suggesting that apoptosis was induced in both NOZ and GR-NOZ cells by the overexpression of miR-451a. Consistent with the suppression of cell growth and morphological changes, western blotting revealed a decrease in cyclin D1, an increase in Bax, a core regulator of the intrinsic apoptotic pathway, and cleaved caspase-3 in both cell lines transfected with the miR-451a mimic (Figure 1F). The increase of annexin V staining, an early marker of apoptosis, was also observed in these cells, with no difference in a marker of necrosis (Figure 1G). These findings revealed that miR-451a inhibits cell proliferation and viability by inducing apoptosis in NOZ and GR-NOZ cells.

miR-451a inhibits the PI3K/AKT signaling pathway partially through the downregulation of MIF in NOZ and GR-NOZ cells

To address the mechanism by which miR-451a inhibits cell growth in the GBC cell lines, an enrichment analysis of the target genes of miR-451a was performed using the miRNA Pathway Dictionary Database (miRPathDB) and Kyoto Encyclopedia of Genes and Genomes (KEGG) databases. The PI3K/AKT pathway was identified as one of the five most enriched signaling pathways (Figure 2A). Therefore, we evaluated the effects of miR-451a on this pathway in NOZ and GR-NOZ cells.

Overexpression of miR-451a resulted in decreased expression of PI3K and p-Akt (Figure 2B) in both cell lines, along with consistent regulation of downstream modulators, such as cyclin D1 and Bax (Figure 1F). In contrast, PTEN, which negatively regulates the PI3K/AKT signaling pathway, was not affected by miR-451a overexpression. These findings suggest that miR-451a deactivates the PI3K/AKT signaling pathway along with downstream regulation and inhibits cell growth in NOZ and GR-NOZ cells.

According to the miRNA target prediction database (miRDB), *MIF*, a gene known to activate the PI3K/AKT pathway in several cancers,[25,26] is a predicted target gene of miR-451a. Therefore, dual-luciferase reporter assays were performed to investigate whether the 3′-untranslated region (3′-UTR) of *MIF* is a direct target of miR-451a. Co-transfection of NOZ and GR-NOZ cells with wild-type (WT) *MIF* 3′-UTR/pmirGLO and the miR-451a mimic caused a significant decrease in luciferase activity compared with cells transfected with the NC mimic (Figure 2C), suggesting that miR-451a directly targets *MIF* in both GBC cell lines. As expected, reverse transcription-quantitative

Figure 1. MiR-451a inhibits cell proliferation and induces apoptosis in NOZ and GR-NOZ cells

(A) Phase-contrast microscopy images of GBC cell lines, NOZ and GR-NOZ. Scale bar, 200 μm. (B) The IC50 of GEM in NOZ and GR-NOZ cells. (C) Western blotting images of gemcitabine (GEM) resistance-related proteins in NOZ and GR-NOZ cells. (D) The MTT assays showing cell proliferation after the introduction of miR-451a mimic into NOZ and GR-NOZ cells. (E) Hoechst staining images showing apoptotic cells with nuclear condensation after the introduction of miR-451a mimic in NOZ and GR-NOZ cells. Scale bar, 100 μm. (F) Western blotting showing the expression levels of proteins associated with cell proliferation and apoptosis in NOZ and GR-NOZ cells after the introduction of miR-451a. (G) Luminescence and fluorescence measurements for the detection of annexin V and necrosis in NOZ and GR-NOZ cells after the introduction of miR-451a mimic. Data are presented as the mean ± SD. *$p < 0.05$, **$p < 0.01$, ***$p < 0.005$, ****$p < 0.001$.

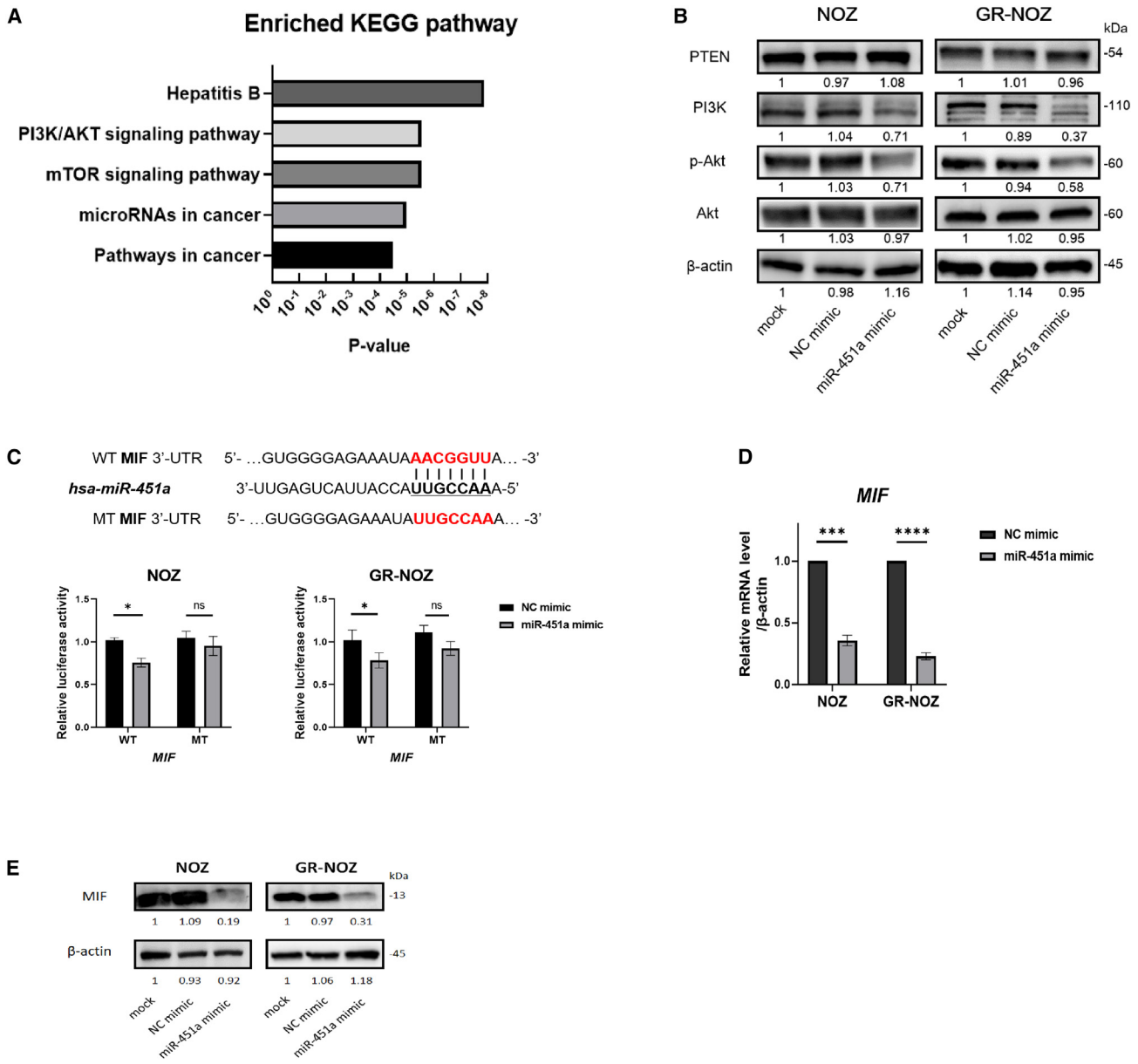

Figure 2. MiR-451a inhibits the PI3K/AKT signaling pathway partially through direct downregulation of MIF in NOZ and GR-NOZ cells

(A) A KEGG pathway analysis of miR-451a using miRPathDB identified the PI3K/AKT signaling pathway as one of the five most highly enriched signaling pathways. (B) Western blotting showing the expression levels of proteins related to the PI3K/AKT signaling pathway. (C) A schematic diagram of miR-451a and *MIF* wild-type (WT) targeting the complementary sequence and *MIF* mutant type (MT). Luciferase reporter assays used vectors containing either *MIF* WT or *MIF* MT sequences of miR-451a target site in NOZ and GR-NOZ cells. (D) The level of *MIF* mRNA expression in miR-451a-transfected NOZ and GR-NOZ cells. (E) Western blotting showing expression levels of MIF in miR-451a-transfected NOZ and GR-NOZ cells. Data are presented as the mean ± SD. *p < 0.05, ***p < 0.005, ****p < 0.001.

polymerase chain reaction (RT-qPCR) and western blotting confirmed that migration inhibitory factor (MIF) expression was markedly decreased in GBC cells transfected with the miR-451a mimic compared with those transfected with the NC mimic (Figures 2D and 2E). These results imply that miR-451a inhibits the PI3K/AKT pathway, to some extent, through downregulating MIF in both NOZ and GR-NOZ cells.

miR-451a reverses epithelial-mesenchymal transitioning and inhibits migration and colony formation in NOZ and GR-NOZ cells

The PI3K/AKT signaling pathway is also involved in epithelial-mesenchymal transitioning (EMT), which plays a significant role in chemoresistance and cancer metastasis. Thus, we examined whether miR-451a regulates the expression of EMT-related mRNAs and proteins and their migratory activities in both GBC cell lines.

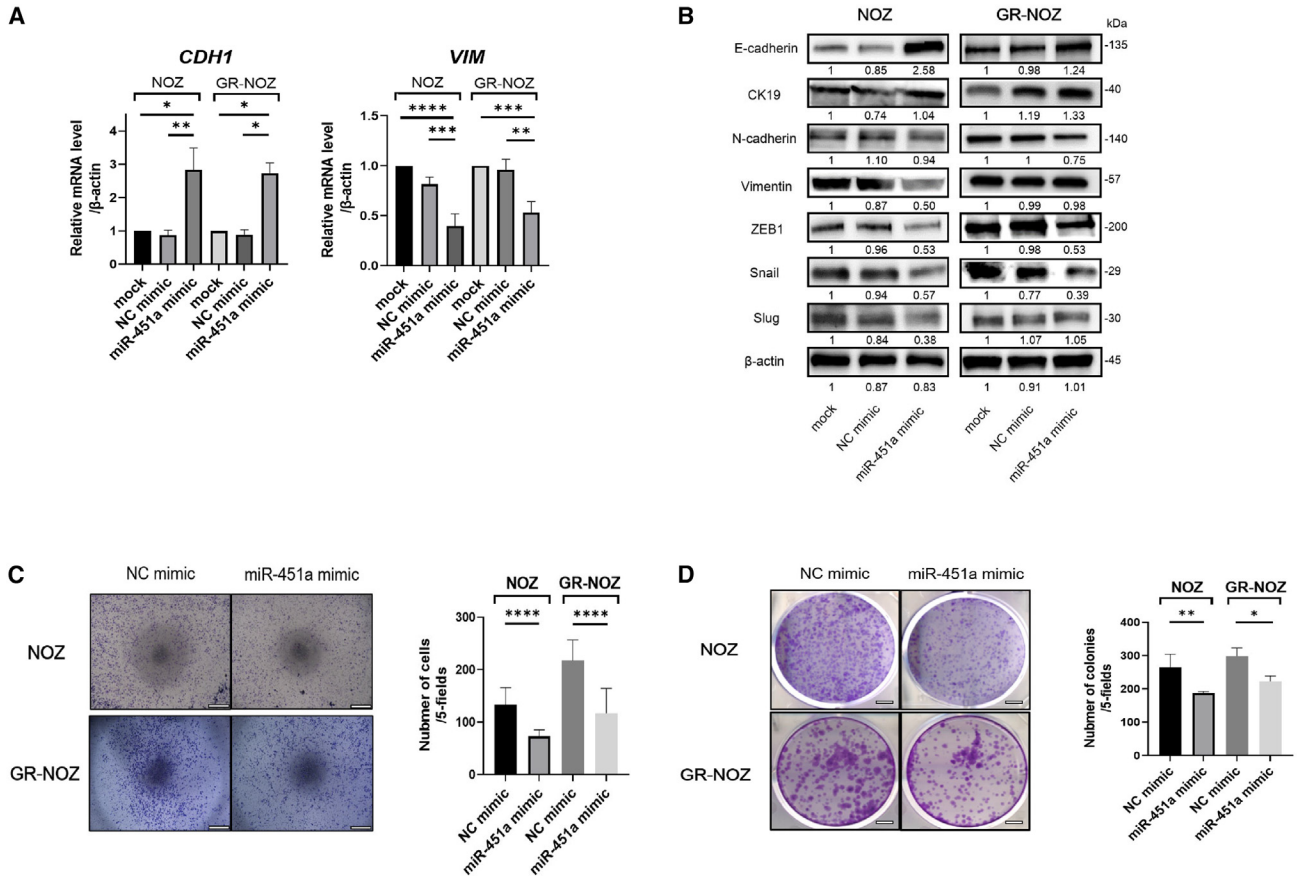

Figure 3. MiR-451a reverses EMT and inhibits migration and colony formation in NOZ and GR-NOZ cells

(A) An RT-qPCR analysis of the expression of *CDH1* and *VIM* in both NOZ and GR-NOZ cells after transfection of miR-451a mimic. (B) Western blotting demonstrating the expression of epithelial protein markers and the mesenchymal protein markers in both cell lines after transfection of miR-451a mimic. (C) Migration ability in miR-451a-transfected NOZ and GR-NOZ cells. Scale bar, 500 μm. (D) Colony formation assays in both cell lines after miR-451a transfection. Scale bar, 5 mm. Data are presented as the mean ± SD. *p < 0.05, **p < 0.01, ***p < 0.005, ****p < 0.001. EMT, epithelial-mesenchymal transition.

RT-qPCR showed that, as a result of miR-451a introduction into the NOZ cell lines, *CDH1* was significantly upregulated ($p < 0.01$), and *VIM* was significantly downregulated ($p < 0.005$), compared with cells transfected with the NC mimic (Figure 3A). In addition, western blotting demonstrated that mesenchymal markers such as N-cadherin, Vimentin, ZEB1, Snail, and Slug were repressed. In contrast, epithelial markers such as E-cadherin and CK19 were elevated (Figure 3B), indicating that miR-451a promoted the mesenchymal-epithelial transition (MET) in the NOZ and GR-NOZ cell lines. The Transwell migration assay revealed that the number of migrated cells was consistently significantly lower after transfection with the miR-451a mimic than with the NC mimic in both cell lines (NOZ, $p < 0.001$; GR-NOZ, $p < 0.001$; Figure 3C). A colony formation assay was performed to confirm the antineoplastic effects of miR-451a on cancer stemness. The number of colonies formed by GBC cells transfected with the miR-451a mimic was significantly lower than that formed by cells transfected with the NC mimic, indicating the potential role of miR-451a in suppressing cancer stemness (NOZ, $p < 0.01$; GR-NOZ, $p < 0.05$; Figure 3D). MiR-451a exhibited an antineoplastic effect by suppressing cell growth, inducing apoptosis, promoting MET, and reducing stem cell capacity, through partial inhibition of the MIF-mediated PI3K/AKT pathway, in NOZ and GR-NOZ cells. These findings suggest that miR-451a is a promising therapeutic target for overcoming GEM-related chemoresistance in GBC.

miR-451a suppresses cell proliferation, induces apoptosis, and inhibits EMT in GR-CCA cells

Further investigation using the Gene Expression Omnibus (GEO) database revealed that miR-451a was the most significantly downregulated miRNA in CCA tissues compared with its expression in normal bile duct tissues (GSE53870; Figures 4A and 4B; Table S1). Therefore, we hypothesized that miR-451a could suppress cell growth and inhibit EMT in CCA. We attempted to validate these antineoplastic effects using two human CCA cell lines, TFK-1 derived from extrahepatic CCA and HuCCT1 derived from intrahepatic CCA.

Based on the IC50 values of GEM, HuCCT1 and TFK-1 cells were considered GR-CCA cell lines (Figure 4C). After the introduction

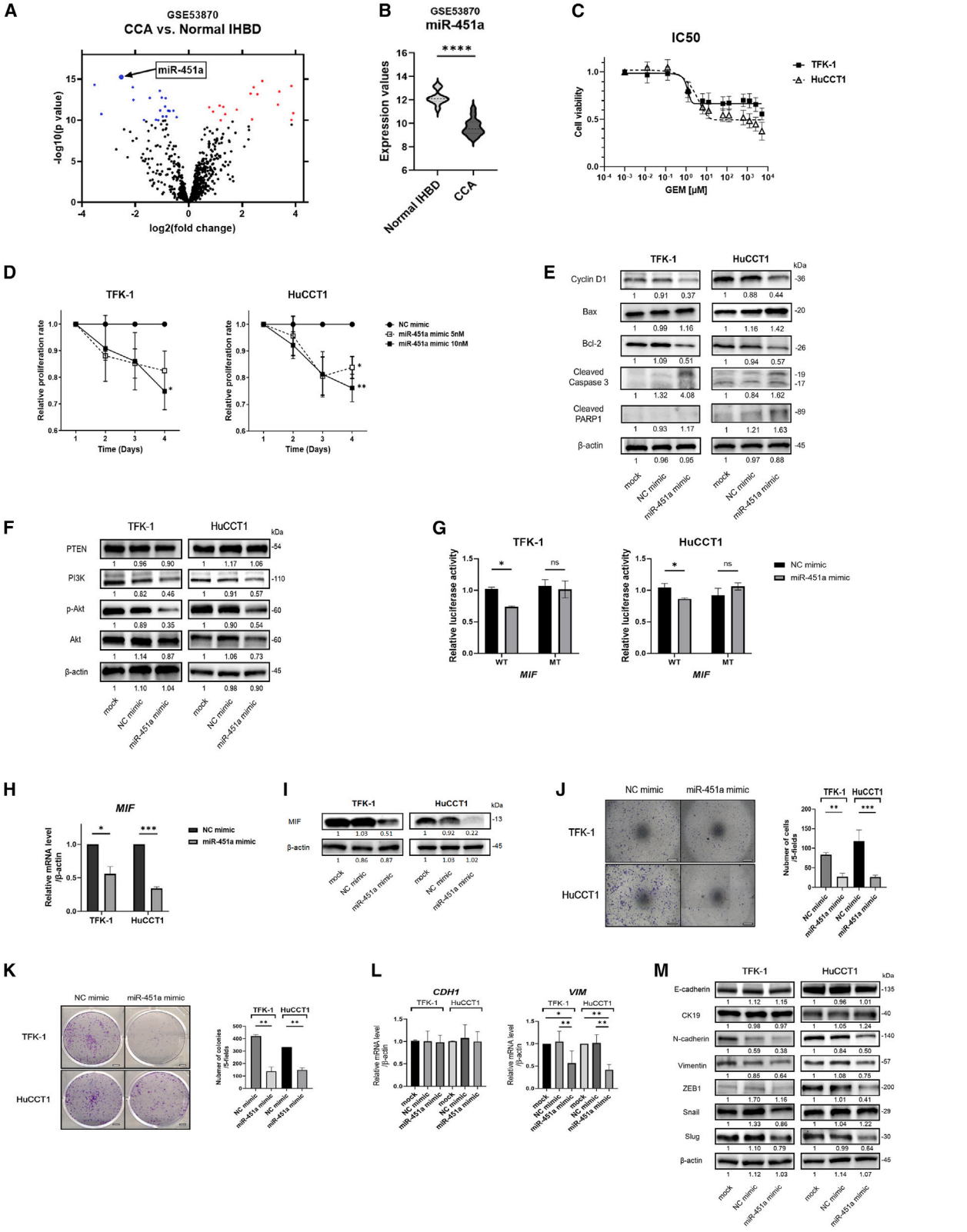

(legend on next page)

of miR-451a, cell proliferation was significantly suppressed in both CCA cell lines compared with that observed after the introduction of the NC mimic (TFK-1, $p < 0.05$; HuCCT1, $p < 0.01$; Figure 4D). This suppressed cell growth was consistent with the downregulation of cyclin D1 and Bcl-2 and upregulation of Bax, cleaved caspase-3, and cleaved Poly (ADP-ribose) polymerase-1 (PARP1), which suggested apoptosis induction (Figure 4E). In addition, these tumor-suppressor functions were induced by inhibiting the PI3K/AKT pathway, partially through the direct regulation of MIF (Figures 4F–4I), which is generally upregulated in CCA.[19] Furthermore, the migratory ability and stemness capacity were significantly reduced in both TFK-1 and HuCCT1 cells after miR-451a transfection ($p < 0.01$; Figures 4J and 4K). However, RT-qPCR analysis showed that miR-451a significantly decreased *VIM* expression ($p < 0.01$) but did not increase *CDH1* expression (Figure 4L). Consistent with this result, western blot analysis revealed reduced expression levels of Vimentin, N-cadherin, ZEB1, Snail, and Slug but no increase in E-cadherin or CK19 expression. These findings suggest that the complete process of MET[27] did not occur (Figure 4M), unlike the results in GBC cells described above. TFK-1 and HuCCT1 cells naturally express high levels of E-cadherin, and the epithelial-like phenotype of both CCA cell lines makes it challenging to upregulate the expression of epithelial markers (Figure S1).

Therefore, CCA has typically downregulated-miR-451a expression; the introduction of miR-451a can suppress cell proliferation and cell viability and, with apoptosis, may inhibit EMT, suggesting that miR-451a could be a therapeutic target for GR-CCA.

miR-451a inhibits cell viability in a 3D spheroid model of GBC, CCA cell lines, and murine tumorigenic gallbladder-derived organoids

Mimicking *in vivo* conditions, we employed a 3D tumor spheroid model to verify the impact of miR-451a on the viability of BTCs with a complex architecture and elucidate its effect on stem cell properties that cause chemoresistance. For the analysis using this model, two GBC and GR-CCA cell lines and tumorigenic gallbladder-derived organoids mimicking GBC were used.

The 3D cell viability assay demonstrated significant suppression of cell viability in an miR-451a-concentration-dependent manner in NOZ and GR-NOZ spheroids (NOZ, $p < 0.01$; GR-NOZ, $p < 0.05$; Figure 5A), consistent with the effects observed in the 2D cell culture model described above. Additionally, the sphere size associated with the tumor volume was smaller after exposure (Figure 5B). In contrast, cell viability was mildly but significantly suppressed in the TFK-1 and HuCCT1 spheroids ($p < 0.05$).

To confirm the effect of miR-451a on cancer stem cells, a 3D tumor spheroid assay with a gallbladder-derived organoid carcinogenesis model generated from $Kras^{LSL\text{-}G12D/+}$; $Trp53^{f/f}$ mice was used (Figure 5C). Consistent with the lower expression of miR-451a in human resected BTC samples, as shown in Figure 4B, the 3D human BTC-derived organoids had significantly lower levels of miR-451a than the normal bile duct-derived organoids, based on GSE 112408 (Figure 5D). Furthermore, the Cre-induced tumorigenic gallbladder organoids, which mimicked GBC, exhibited lower levels of miR-451a expression and higher levels of MIF than the pLKO.1-induced gallbladder organoids mimicking the normal biliary epithelium (Figure 5E). Consequently, introducing miR-451a into spheroids derived from GBC-mimicking organoids led to significant suppression of cell viability compared with spheroids treated with the NC mimic (Figure 5F), indicating that miR-451a may be effective in inhibiting the growth of GBC from a stemness perspective.

DISCUSSION

This study revealed that miR-451a inhibited cell proliferation and promoted apoptosis and MET in GBC cell lines, regardless of the GEM resistance status. Direct downregulation of MIF, one of the targets of miR-451a, and deactivation of the downstream PI3K/AKT signaling pathway may be involved in these mechanisms. In addition, miR-451a was found to be the most downregulated miRNA in CCA using *in silico* analysis, and a similar antineoplastic effect to what was seen in the GBC cell lines was observed in GR-CCA cell lines upon miR-451a transfection. Based on the suppression of cell viability and reduction of stem cell properties observed in the 3D tumor spheroid model that mimics *in vivo* conditions, our study suggests that miR-451a replacement therapy may be a potential strategy for BTCs, even after acquiring GEM resistance.

Our previous study identified miR-451a as a potential therapeutic target for GBC by analyzing serum EVs from patients.[19] MIF, a miR-451a target, is a pro-inflammatory cytokine that supports the development of neoplasms, including malignant transformation, carcinogenesis, tumor growth, viability, and angiogenesis,[28–30] and is overexpressed in several types of cancer.[31–33] MIF directly promotes cell survival by

Figure 4. MiR-451a suppresses cell proliferation, induces apoptosis, and inhibits EMT in distal and intrahepatic GR-CCA cells

(A) Volcano plot of miRNA expression in cholangiocarcinoma (CCA) using GSE53870 from the Gene Expression Omnibus dataset. The horizontal axis represents the fold change, and the vertical axis represents the p value (−log10). miR-451a was the most significantly downregulated miRNA in CCA tissue compared with its relative expression in normal intrahepatic bile duct (IHBD) tissue. (B) Expression levels of miR-451a in CCA tissues and normal IHBD tissues using the same database. (C) The IC50 of GEM in both CCA cell lines, TFK-1 and HuCCT1. (D) An MTT assay showing cell proliferation after the introduction of miR-451a mimic into TFK-1 and HuCCT1 cells. (E and F) Western blot showing the expression levels of proteins associated with cell cycles and apoptosis, and those related to the PI3K/AKT signaling pathway in TFK-1 and HuCCT1 cells after the introduction of miR-451a. (G) Luciferase reporter assays used vectors containing either *MIF* WT or *MIF* MT sequences of the miR-451a target site in TFK-1 and HuCCT1 cells. (H) The mRNA expression levels of *MIF* in miR-451a-transfected TFK-1 and HuCCT1 cells. (I) Western blotting showing the expression levels of MIF in these cells. (J) Migration ability in miR-451a-transfected TFK-1 and HuCCT1 cells. Scale bar, 500 μm. (K) Colony formation assays in both cell lines after miR-451a transfection. Scale bar, 5 mm. (L and M) RT-qPCR and western blotting analyses showing the expression of epithelial and mesenchymal markers in both cell lines after transfection of miR-451a mimic. Data are presented as the mean ± SD. *$p < 0.05$, **$p < 0.01$, ***$p < 0.005$, ****$p < 0.001$. EMT, epithelial-mesenchymal transition.

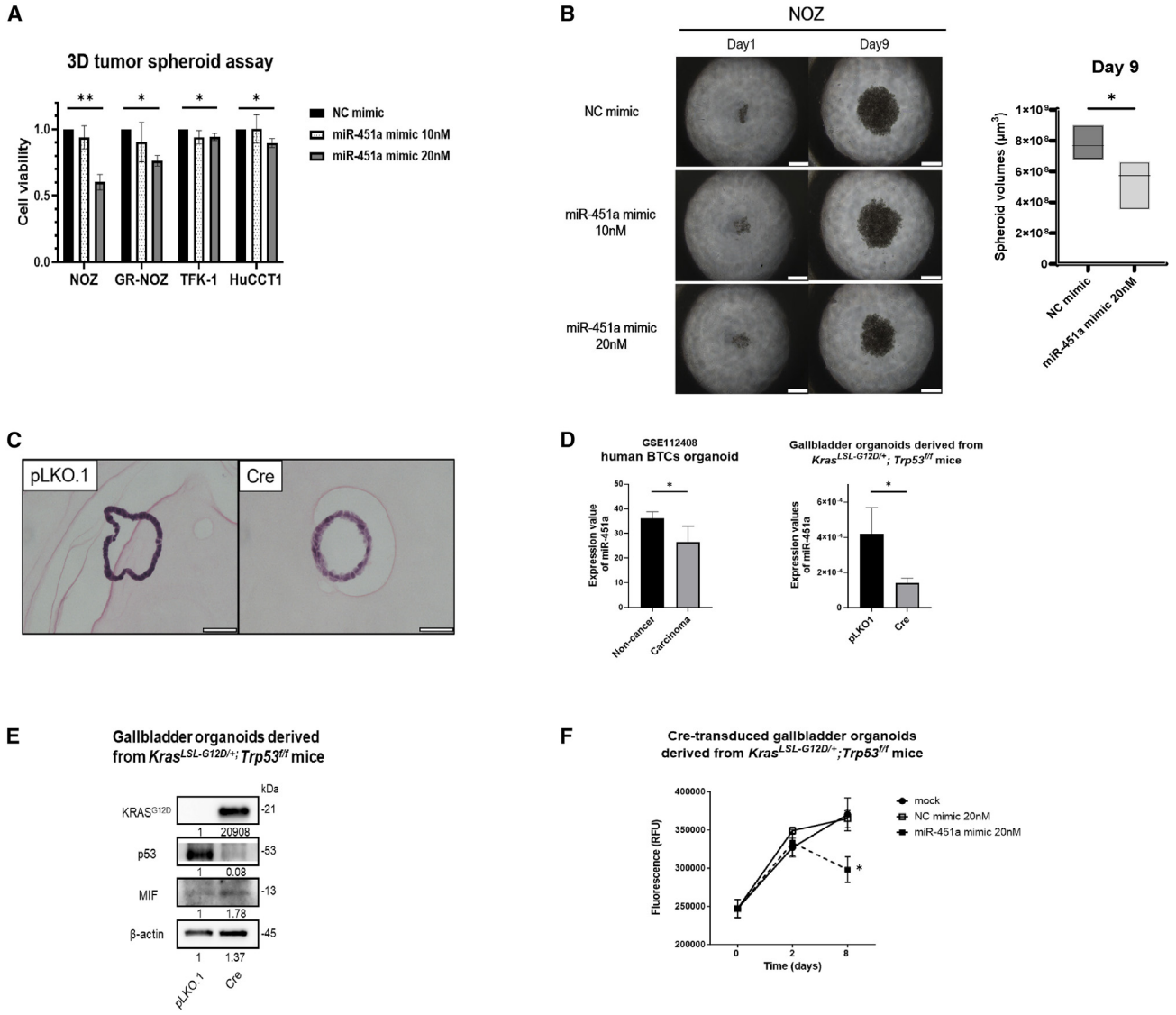

Figure 5. MiR-451a inhibits cell viability of BTCs in the 3D tumor spheroid model mimicking *in vivo* conditions

(A) Cell proliferation capacity after transfection of miR-451a into the tumor spheroids of biliary tract cancer (BTC) cell lines, including NOZ, GR-NOZ, TFK-1, and HuCCT1, determined by an ATP-based assay. (B) Measurement of spheroid volumes in NOZ spheres after the transfection of miR-451a mimic using microscopic images (days 1 and 9). Scale bar, 500 μm. Spheroid volumes on day 9 are indicated in the right panel. (C) Morphology of pLKO.1- and Cre-induced gallbladder organoids derived from *Kras*$^{LSL\text{-}G12D/+}$; *Trp53*$^{f/f}$ mice. Scale bar, 50 μm. (D) The expression levels of miR-451a in human BTC-derived 3D organoids and normal cholangiocyte-derived organoids (GSE112408). Among the gallbladder organoids generated from *Kras*$^{LSL\text{-}G12D/+}$; *Trp53*$^{f/f}$ mice, miR-451a expression was significantly lower in Cre-induced tumorigenic organoids than in pLKO.1-induced organoids as well. (E) Western blotting images showing the MIF expression in Cre-induced tumorigenic gallbladder organoids and pLKO.1-induced organoids. (F) Cell growth capacity after transfection of miR-451a into Cre-induced tumorigenic gallbladder organoids derived from *Kras*$^{LSL\text{-}G12D/+}$; *Trp53*$^{f/f}$ mice using the 3D tumor spheroid model. Data are presented as the mean ± SD. *p < 0.05, **p < 0.01.

activating the PI3K/AKT pathway,[25,26] a principally activated signaling pathway in BTCs,[34,35] and this activation can also be triggered by mutations in the *PIK3CA* gene, a key driver of BTCs.[6] Furthermore, MIF also activates the ERK1/2 and AMPK pathways.[36] Notably, these processes have been shown to potentiate metastasis and increase the resistance to chemotherapy, particularly in GBC[37] and CCA.[34,35] Li et al. reported that the positive staining rate of PI3K in GBC tissue was significantly higher than that in peritumoral tissue (50% vs. 10%, $p < 0.01$) and significantly higher in poorly differentiated adenocarcinoma than in well-differentiated adenocarcinoma ($p < 0.01$).[38] Furthermore, increased PI3K expression is associated with decreased overall survival (OS) in patients with GBC. Similarly, it has been reported that patients with CCA with low PTEN expression had significantly reduced OS than those with high PTEN expression ($p < 0.05$).[39]

Recently, a second-phase study on copanlisib, a PI3K inhibitor, was conducted for advanced/unresectable BTC.[40] Adding copanlisib to GEM and cisplatin resulted in a more prolonged progression-free survival and OS in the population with a loss of PTEN expression, approximately 70% in BTC. In contrast, we demonstrated that miR-451a inhibited the PI3K/AKT pathway partially through the downregulation of MIF in even GEM-resistant BTCs, in a PTEN-independent manner. Moreover, miR-451a may inhibit the AKT/Cyclin D1 signaling pathway[41–43] and other MIF-mediated pathways. Thus, miR-451a replacement therapy may be a strategy for suppressing cancer growth in patients with refractory BTC.

To overcome chemoresistance and metastasis in cancer, it is crucial to focus on EMT, a major strategy by which cancer cells acquire a stem cell phenotype.[44,45] Our study found that miR-451a induces MET in GBC cells, irrespective of GEM resistance. The PI3K/AKT pathway regulates EMT via Snail and is pivotal for cancer stem cell maintenance and survival.[46] Additionally, miR-451a-targeted c-Myc affects EMT,[47] and c-Myc's high expression is associated with chemoresistance in other cancer types.[48] While other signaling pathways such as Notch, Wnt/beta-catenin, and TGF-beta/Smad also contribute to EMT programming,[49–52] our results demonstrated that miR-451a inhibited EMT and stem cell growth, partially through PI3K/AKT pathway deactivation and presumably via c-Myc regulation (Figure S2).[22,46,53–55] These findings indicate that miR-451a lessens chemoresistance in GEM-refractory BTCs. Furthermore, combining miR-451a with chemotherapeutic agents may reduce chemoresistance and provide long-term antineoplastic effects.[56] However, further analysis is required.

Supplementation of miRNAs is considered a promising target therapy for cancer as well as several diseases, with ongoing clinical trials for several miRNAs.[18,57–59] An ideal drug delivery system (DDS) should have efficient delivery, high cellular uptake and stability, and specific delivery to tumors while minimizing non-specific delivery to normal tissues, systemic immune responses, and immunotoxicity.[18,60] An ideal DDS for miRNAs has yet to be established, although progress has been made toward targeted vehicle-free delivery approaches.[61] Thus, in this study, to investigate the potential for further clinical applications of miR-451a, a 3D tumor spheroid culture model composed of cells in different proliferative and metabolic states[62–64] was employed. The model confirmed the significant antineoplastic effects of miR-451a in BTCs. Additionally, Cre-induced gallbladder organoids generated from *Kras*$^{LSL\text{-}G12D/+}$; *Trp53*$^{f/f}$ mice mimicking GBC demonstrated the growth inhibition of stem cells after miR-451a introduction. Our study highlights miR-451a as a potential target for overcoming refractory BTCs. In the era of the current combining immunotherapy with chemotherapy for BTCs,[8] nucleic acid-based therapy might not be an immediate first-line treatment. However, as we have suggested its potential as a treatment following GEM resistance, further developments as a later regimen are anticipated. Nonetheless, the development of DDS of nucleic acids that effectively and exclusively target the tumor through local or systemic administration and further preclinical studies are needed to develop realistic clinical applications. Since miR-451a has been reported to be involved in erythropoiesis,[65] local administration guided by ultrasonography or endoscopic ultrasonography may benefit cancer treatment.

In conclusion, our study demonstrated that miR-451a regulates the PI3K/AKT pathway by targeting MIF and suppressing cell proliferation, viability, and migration in human GBC and CCA, even with GEM resistance. These results suggest that miRNA-based therapy is a promising treatment option for BTCs for which few effective drugs are currently available. However, further *in vivo* studies and the development of an effective DDS are required to validate the clinical application of miR-451a replacement therapy. Overall, our findings provide insights into a therapeutic strategy for treating BTCs with poor prognosis.

MATERIALS AND METHODS

Cell culture and organoids

Three human BTC cell lines were used in the present study. The GBC cell line, NOZ, was obtained from the JCRB Cell Bank (National Institutes of Biomedical Innovation, Health and Nutrition, Osaka, Japan). This cell line was established by Dr. S. Nagamori (National Institute of Infectious Diseases). Both CCA cell lines, TFK-1 (extrahepatic) and HuCCT1 (intrahepatic), were purchased from the Tohoku University Cell Resource Center (Sendai, Japan). NOZ cells were cultured in William's E Medium (Thermo Fisher Scientific, Waltham, MA, USA) supplemented with 10% FBS and L-glutamine, whereas TFK-1 and HuCCT1 cells were cultured in RPMI-1640 medium (Thermo Fisher Scientific) supplemented with 10% FBS. The cells were grown in a humidified atmosphere containing 5% CO_2 at 37°C. GR-NOZ cells were established by exposure to graded concentrations (12.5–625 nM) of GEM for 4 months. Cell viability was confirmed by determining the IC50, and the expression of two GEM-related proteins, hENT1 and dCK, which play critical roles in the intracellular transport and activation of GEM,[66] respectively, was measured.

Cre- and pLKO.1-transduced gallbladder organoids derived from *Kras*$^{LSL\text{-}G12D/+}$; *Trp53*$^{f/f}$ mice were a gift from Dr. Y. Hippo (Chiba Cancer Center Research Institute, Chiba, Japan).[67] Advanced DMEM/F12 (Thermo Fisher Scientific) containing L-glutamine, penicillin, streptomycin, and amphotericin B, supplemented with 50 ng/mL epidermal growth factor (Peprotech, Rocky Hill, NJ, USA), 100 ng/mL Noggin (Peprotech), 1 μM Jagged1 (AnaSpec, Fremont, CA, USA), and 10 μM Y27632 (Wako, Osaka, Japan) was used with the Matrigel to culture organoids. The Cre-transduced gallbladder organoids demonstrated tumorigenicity after subcutaneous inoculation into nude mice, after which aggressively growing nodules were observed. This study used tumor-derived organoids that mimicked GBC as Cre-transduced gallbladder organoids.

Transfection of miRNA mimic

For gain-of-function experiments on miR-451a, hsa-miR-451a mimics, and mmu-miR-451a mimics (mirVana miRNA mimics, [MC10286], Thermo Fisher Scientific) were transfected into cells using Opti-MEM (Thermo Fisher Scientific) and Lipofectamine

RNAiMAX Transfection Reagent (Invitrogen, Carlsbad, CA, USA). Non-targeting mimics (NC #1; mirVana miRNA mimics, 4464078; Thermo Fisher Scientific) were used as controls in the miRNA mimic experiments. Cell lines were seeded at a concentration of 5×10^4 cells/well in six-well plates or 1.2×10^4 cells/well in 24-well plates, pre-cultured to 60% confluency, and then transfected with the 5, 10, or 20 nM of mimic for 48 h or 72 h, following the manufacturer's protocol.

Cell proliferation and viability assay for 2D cell culture or 3D tumor spheroid model

For 2D cell culture, cell proliferation and viability were measured using the MTT (3-[4,5-dimethylthiazol-2-yl]-2,5 diphenyltetrazolium bromide) assay. Briefly, cells were seeded at a density of 3×10^3 cells/well in 96-well plates and cultured in an incubator. After 24, 48, 72, and 96 h of incubation, MTT was added to each well, and the cells were incubated at 37°C for 3 h. Formazan precipitate was dissolved in dimethyl sulfoxide, and absorbance was measured at 570 nm using a microplate reader (MULTISKAN GO; Thermo Fisher Scientific). Media containing the MTT reagent without cells were used as a blank control. All experiments were performed a minimum of three times.

Cell viability for the 3D tumor spheroid model was analyzed using the CellTiter-Glo 3D Cell Viability Assay (Promega, Madison, WI, USA). Briefly, 1×10^3 or 2×10^3 cells were plated in 96-well ultra-low attachment spheroid plates (#4515; Corning Inc., Corning, NY, USA) to generate tumor spheroids. Two days later, 10 or 20 nM of either the miR-451a mimic or NC mimic was transfected into spheroids composed of BTC cells or Cre-transduced gallbladder organoids. Cell viability was analyzed three times (0, 3, and 8–9 days) using a GloMax Discover Microplate Reader (Promega). Spheroid volume was calculated using the microscopic images, based on the measured major axis (length) and minor axis (width) (Volume [μm^3] = 0.5 × Length [μm] × Width [$\mu m]^2$).[68]

Apoptosis assay

Cells (2×10^5 cells/well) were seeded in six-well plates and incubated for 24 h. The cells were treated with the 10 nM of miR-451a mimic or NC mimic for 72 h. Hoechst 33342 (5 μg/mL; H3570, Invitrogen) was added, and the medium was incubated in the dark for 10 min. The apoptotic cells exhibiting nuclear condensation, which can be used to distinguish apoptotic cells from healthy cells or necrotic cells,[69] were counted under a fluorescence microscope (FSX100, Olympus, Tokyo, Japan), and the average percentage of apoptotic cells in five random high-power fields was calculated.

Additionally, a luminescent apoptosis assay was performed to observe an early marker of apoptosis, annexin V staining. GBC cells suspended in 150 μL media were seeded at a density of 3×10^3 cells per well into Falcon 96-well White/Clear Bottom TC-treated Polystyrene Microplates (#353377, Corning Inc.) and incubated for 24–48 h in a humidified atmosphere containing 5% CO_2 at 37°C. These cells were then transfected with miR-451a mimic and NC mimic, as described above, and were subjected to analysis using the Real Time-Glo Annexin V apoptosis and Necrosis reagent (#JA1011, Promega) according to the manufacturer's instructions. Luminescent and fluorescent signals were monitored over a 48-h period using the GloMax Discover Microplate Reader (Promega).

RT-qPCR

Total RNA was extracted from the cells using a miRNeasy Micro Kit (Qiagen, Valencia, CA, USA) according to the manufacturer's instructions. The samples were reverse-transcribed using Transcriptor Universal cDNA Master Mix (Roche, Basel, Switzerland), and RT-qPCR was performed using the LightCycler 480 SYBR Green I Master Mix (Roche) and LightCycler 96 Real-Time PCR System (Roche) in 96-well plates. The thermocycling conditions were as follows: (1) Pre-denaturation at 95°C for 300 s; (2) cycle reaction (40 times) at 95°C for 10 s, at 60°C for 20 s, and at 72°C for 6 s; and melting curve: 95°C for 5 s, 65°C for 60 s, and 97°C for 4 s. Amplification curves were analyzed using Roche LC 96 software v. 1.1, and the analysis of relative gene expression data were calculated using the $2-\Delta\Delta Cq$ method.[70] All reactions were performed in duplicate. The results were normalized to β-actin expression levels.

The forward and reverse primers used for each gene were as follows: *MIF*, 5′- ACAGCATCGGCAAGATCGG-3′ and 5′- TAATAGTTGATGTAGACCCTGTCCG-3′; *CDH1*, 5′-TCACAGCAGAACTAACACACGG-3′ and 5′-TCAAAATGATAGATTCTTGGGTTGGG-3′; *VIM*, 5′-GGACCAGCTAACCAACGACA-3′ and 5′-TCCTCCTGCAATCCCG-3′; and *β-actin*, 5′-CCTGGCACCCAGCACAAT-3′ and 5′-GCCGATCCACACGGAGTACT-3′.

Western blotting

After transfection with the miR-451a and NC mimics for 48 or 72 h, protein lysates were harvested using radioimmunoprecipitation assay (RIPA) buffer (89900; Thermo Fisher Scientific) with protease inhibitors. The BCA method (23225; Thermo Fisher Scientific) was used to measure the protein concentration. Proteins (10 μg) were resolved by sodium dodecyl sulfate-polyacrylamide gel electrophoresis (SDS-PAGE) and transferred onto polyvinylidene fluoride (PVDF) membranes (Bio-Rad, Hercules, CA, USA). The membranes were blocked using a PVDF blocking reagent (Toyobo, Osaka, Japan) or 2% skimmed milk for 1 h. The primary and secondary antibodies were diluted to 1:2,000 and 1:4,000, respectively. Reactive bands were detected using Clarity Western ECL Substrate (#1705060; Bio-Rad) and ImageQuant LAS 4000 (GE Healthcare Bio-Sciences AB, Uppsala, Sweden). The signal intensity of the band was determined using ImageJ software (version 1.50, NIH, USA).

The primary antibodies used in the study were as follows: Bax (#5023), Bcl-2 (#2876), Cleaved Caspase-3 (#9661), phosphatidylinositol 3-kinase (PI3K) p110α (#4249), Akt (#9272), Phospho-Akt (p-Akt; #4060), Cyclin D1 (#2922), PTEN (#9552), c-Myc (#5605), E-cadherin (#3195), N-cadherin (#13116), Vimentin (#5741), ZEB1 (#3396), Snail (#3879), Slug (#9585), β-actin (#4967; all from Cell Signaling Technology [CST], Danvers, MA, USA), ENT1 (sc-377283), dCK (sc-393099), cleaved PARP1 (sc-56196), macrophage

MIF (sc-271631; both from Santa Cruz Biotechnology, Dallas, TX, USA), and Cytokeratin 19 (CK19; ab15463; Abcam, Cambridge, UK). Horseradish peroxidase (HRP)-conjugated anti-mouse (#7076) and anti-rabbit (#7074; both from CST) antibodies were used as secondary antibodies. All experiments were performed in triplicate.

Migration assay

Transwell migration assays were conducted using an 8-μm pore, 24-well Falcon Cell Culture Insert (Corning Inc.). First, cells were transfected with the miR-451a mimic or NC mimic and cultured for 48 h. Then, 40,000 cells per insert were seeded in serum-free medium while 500 μL medium containing 10% FBS was added to the bottom chamber, and cellular migration was assessed 16 h after seeding. Cells that migrated to the lower surface of the inserts were fixed with 4% paraformaldehyde (PFA), stained with 0.5% crystal violet, and counted in five random high-power fields under an inverted microscope (CKX41, Olympus, Tokyo, Japan). All experiments were performed in triplicate.

Colony formation assay

Cells were transfected with a miR-451a mimic or NC mimic and cultured for 48 h, after which the transfected cells were seeded into six-well plates at a density of 3×10^3 cells/well. After culturing for 10 days, the cells were fixed using 4% PFA and stained with 0.5% crystal violet. Colonies containing >50 cells were counted under the inverted microscope (Olympus).

Dual-luciferase reporter assay

Plasmids were constructed using the pmirGLO Dual-Luciferase miRNA Target Expression Vector (Promega) for the binding site in the 3′-UTR of the mRNA of the potential target gene (*MIF*), based on the miRDB.[71] For the reported gene assay, NOZ, GR-NOZ, TFK-1, and HuCCT1 cells were co-transfected with reporter vectors (*MIF* WT or *MIF* mutant type [MT]), miR-451a mimics, and NC mimics using Lipofectamine 3000 Reagent (Invitrogen). Forty-eight hours after transfection, luciferase activity was evaluated using the Nano-Glo Dual-Luciferase Reporter Gene Assay System (Promega) and a GloMax Discover Microplate Reader (Promega). Normalization was performed by comparison with Renilla luciferase activity.

Bioinformatics analysis

The GEO datasets GSE53870 (miRNA profile of human intrahepatic CCA) and GSE112408 (miRNA profiles of organoids derived from human BTCs) were used to determine the miRNA expression in human tissues and organoids. The miRNAs of interest were analyzed to determine their expression levels in malignant tissues, including CCA, GBC, and normal tissues, using GEO2R, an online analysis tool in the GEO database. The predicted miRNA targets were identified using miRDB. The KEGG pathway and the miRPathDB, one of the most comprehensive and advanced resources for miRNAs and their target pathways, were also used.[72]

Statistical analysis and data processing

All statistical analyses and IC50 calculations were performed using JMP v. 15.0 (SAS Institute Inc., Cary, NC, USA) and GraphPad Prism v. 9.3 (GraphPad Software Inc., La Jolla, CA, USA). IC50 values were calculated using a nonlinear regression model. Comparisons between groups were performed using the Kruskal-Wallis, Mann-Whitney *U*, Pearson's chi-square, or Wilcoxon rank-sum tests. As we summarized the data by adjusting the values from NC as 1, no error bar exists in the NCs for the relative quantitative assessment of cell proliferation and viability and RT-qPCR. All the tests were two-sided. Statistical significance was set at $p < 0.05$.

DATA AND CODE AVAILABILITY

The data generated in this study are available upon request from the corresponding author.

SUPPLEMENTAL INFORMATION

Supplemental information can be found online at https://doi.org/10.1016/j.omtn.2023.102054.

ACKNOWLEDGMENTS

We thank Dr. Yoshitaka Hippo (Chiba Cancer Center Research Institute, Chiba, Japan) for providing the Cre- and pLKO.1-transduced gallbladder organoids derived from *Kras*$^{LSL\text{-}G12D/+}$; *Trp53*$^{f/f}$ mice. We also thank Ms. Yuki Osaki for her technical support. This work was financially supported in part by JSPS KAKENHI (Grant Numbers 21K07962 and 22K08032 to K.T.) from the Japan Society for the Promotion of Science, and Okayama Health Foundation Cancer Research Grants (to K.T.).

AUTHOR CONTRIBUTIONS

Writing – Original draft, and Methodology, T.Obata and K.T.; Conceptualization and Funding acquisition, K.T.; Resources, and Investigation, T.Obata, K.T., E.U., T.Oda, T.K., S.A., Y.F., T.Y., D.U., K.M., S.H., H.K., H.O., and M.O.; Formal analysis, T.Obata, K.T., and E.U.; Writing – Review & Editing, T.Obata, K.T., T.Oda, T.K., S.A., Y.F., T.Y., D.U., K.M., S.H., H.K., H.O., and M.O.; Supervision, K.T., H.O., and M.O.

DECLARATION OF INTERESTS

The authors declare no competing interests.

REFERENCES

1. Valle, J.W., Kelley, R.K., Nervi, B., Oh, D.Y., and Zhu, A.X. (2021). Biliary tract cancer. Lancet *397*, 428–444.
2. Sung, H., Ferlay, J., Siegel, R.L., Laversanne, M., Soerjomataram, I., Jemal, A., and Bray, F. (2021). Global Cancer Statistics 2020: GLOBOCAN Estimates of Incidence and Mortality Worldwide for 36 Cancers in 185 Countries. CA. Cancer J. Clin. *71*, 209–249.
3. Banales, J.M., Marin, J.J.G., Lamarca, A., Rodrigues, P.M., Khan, S.A., Roberts, L.R., Cardinale, V., Carpino, G., Andersen, J.B., Braconi, C., et al. (2020). Cholangiocarcinoma 2020: the next horizon in mechanisms and management. Nat. Rev. Gastroenterol. Hepatol. *17*, 557–588.
4. Valle, J.W., Borbath, I., Khan, S.A., Huguet, F., Gruenberger, T., and Arnold, D.; ESMO Guidelines Committee (2016). Biliary cancer: ESMO Clinical Practice Guidelines for diagnosis, treatment and follow-up. Ann. Oncol. *27*, v28–v37.
5. Lamarca, A., Edeline, J., and Goyal, L. (2022). How I treat biliary tract cancer. ESMO open *7*, 100378.
6. Patel, T. (2011). Cholangiocarcinoma–controversies and challenges. Nat. Rev. Gastroenterol. Hepatol. *8*, 189–200.

7. Valle, J., Wasan, H., Palmer, D.H., Cunningham, D., Anthoney, A., Maraveyas, A., Madhusudan, S., Iveson, T., Hughes, S., Pereira, S.P., et al. (2010). Cisplatin plus gemcitabine versus gemcitabine for biliary tract cancer. N. Engl. J. Med. *362*, 1273–1281.
8. Oh, D.Y., He, A.R., Qin, S., Chen, L.T., Okusaka, T., Vogel, A., Kim, J.W., Suksomboon charoen, T., Lee, M.A., Kitano, M., et al. (2022). Durvalumab plus Gemcitabine and Cisplatin in Advanced Biliary Tract Cancer. NEJM Evid *1*, EVIDoa2200015.
9. Lamarca, A., Palmer, D.H., Wasan, H.S., Ross, P.J., Ma, Y.T., Arora, A., Falk, S., Gillmore, R., Wadsley, J., Patel, K., et al. (2021). Second-line FOLFOX chemotherapy versus active symptom control for advanced biliary tract cancer (ABC-06): a phase 3, open-label, randomised, controlled trial. Lancet Oncol. *22*, 690–701.
10. Nakamura, H., Arai, Y., Totoki, Y., Shirota, T., Elzawahry, A., Kato, M., Hama, N., Hosoda, F., Urushidate, T., Ohashi, S., et al. (2015). Genomic spectra of biliary tract cancer. Nat. Genet. *47*, 1003–1010.
11. Kulkarni, J.A., Witzigmann, D., Thomson, S.B., Chen, S., Leavitt, B.R., Cullis, P.R., and van der Meel, R. (2021). The current landscape of nucleic acid therapeutics. Nat. Nanotechnol. *16*, 630–643.
12. Lee, Y.S., and Dutta, A. (2009). MicroRNAs in cancer. Annu. Rev. Pathol. *4*, 199–227.
13. Peng, Y., and Croce, C.M. (2016). The role of MicroRNAs in human cancer. Signal Transduct. Target. Ther. *1*, 15004.
14. Hussen, B.M., Hidayat, H.J., Salihi, A., Sabir, D.K., Taheri, M., and Ghafouri-Fard, S. (2021). MicroRNA: A signature for cancer progression. Biomed. Pharmacother. *138*, 111528.
15. Calin, G.A., and Croce, C.M. (2006). MicroRNA signatures in human cancers. Nat. Rev. Cancer *6*, 857–866.
16. Kozomara, A., Birgaoanu, M., and Griffiths-Jones, S. (2019). miRBase: from microRNA sequences to function. Nucleic Acids Res. *47*, D155–D162.
17. Bader, A.G., Brown, D., and Winkler, M. (2010). The promise of microRNA replacement therapy. Cancer Res. *70*, 7027–7030.
18. Rupaimoole, R., and Slack, F.J. (2017). MicroRNA therapeutics: towards a new era for the management of cancer and other diseases. Nat. Rev. Drug Discov. *16*, 203–222.
19. Ueta, E., Tsutsumi, K., Kato, H., Matsushita, H., Shiraha, H., Fujii, M., Matsumoto, K., Horiguchi, S., and Okada, H. (2021). Extracellular vesicle-shuttled miRNAs as a diagnostic and prognostic biomarker and their potential roles in gallbladder cancer patients. Sci. Rep. *11*, 12298.
20. Théry, C., Zitvogel, L., and Amigorena, S. (2002). Exosomes: Composition, biogenesis and function. Nat. Rev. Immunol. *2*, 569–579.
21. Pan, X., Wang, R., and Wang, Z.X. (2013). The potential role of miR-451 in cancer diagnosis, prognosis, and therapy. Mol. Cancer Ther. *12*, 1153–1162.
22. Wang, R., Wang, Z.X., Yang, J.S., Pan, X., De, W., and Chen, L.B. (2011). MicroRNA-451 functions as a tumor suppressor in human non-small cell lung cancer by targeting ras-related protein 14 (RAB14). Oncogene *30*, 2644–2658.
23. Zhao, J., Li, H., Zhao, S., Wang, E., Zhu, J., Feng, D., Zhu, Y., Dou, W., Fan, Q., Hu, J., et al. (2021). Epigenetic silencing of miR-144/451a cluster contributes to HCC progression via paracrine HGF/MIF-mediated TAM remodeling. Mol. Cancer *20*, 46.
24. Yamada, Y., Arai, T., Sugawara, S., Okato, A., Kato, M., Kojima, S., Yamazaki, K., Naya, Y., Ichikawa, T., and Seki, N. (2018). Impact of novel oncogenic pathways regulated by antitumor miR-451a in renal cell carcinoma. Cancer Sci. *109*, 1239–1253.
25. Lue, H., Thiele, M., Franz, J., Dahl, E., Speckgens, S., Leng, L., Fingerle-Rowson, G., Bucala, R., Lüscher, B., and Bernhagen, J. (2007). Macrophage. Macrophage migration inhibitory factor (MIF) promotes cell survival by activation of the Akt pathway and role for CSN5/JAB1 in the control of autocrine MIF activity. Oncogene *26*, 5046–5059.
26. Oliveira, C.S., de Bock, C.E., Molloy, T.J., Sadeqzadeh, E., Geng, X.Y., Hersey, P., Zhang, X.D., and Thorne, R.F. (2014). Macrophage migration inhibitory factor engages PI3K/Akt signalling and is a prognostic factor in metastatic melanoma. BMC Cancer *14*, 630.
27. Aiello, N.M., Maddipati, R., Norgard, R.J., Balli, D., Li, J., Yuan, S., Yamazoe, T., Black, T., Sahmoud, A., Furth, E.E., et al. (2018). EMT Subtype Influences Epithelial Plasticity and Mode of Cell Migration. Dev. Cell *45*, 681–695.e4.
28. Fingerle-Rowson, G., Petrenko, O., Metz, C.N., Forsthuber, T.G., Mitchell, R., Huss, R., Moll, U., Müller, W., and Bucala, R. (2003). The p53-dependent effects of macrophage migration inhibitory factor revealed by gene targeting. Proc. Natl. Acad. Sci. USA *100*, 9354–9359.
29. Petrenko, O., Fingerle-Rowson, G., Peng, T., Mitchell, R.A., and Metz, C.N. (2003). Macrophage migration inhibitory factor deficiency is associated with altered cell growth and reduced susceptibility to Ras-mediated transformation. J. Biol. Chem. *278*, 11078–11085.
30. Wilson, J.M., Coletta, P.L., Cuthbert, R.J., Scott, N., MacLennan, K., Hawcroft, G., Leng, L., Lubetsky, J.B., Jin, K.K., Lolis, E., et al. (2005). Macrophage migration inhibitory factor promotes intestinal tumorigenesis. Gastroenterology *129*, 1485–1503.
31. Funamizu, N., Hu, C., Lacy, C., Schetter, A., Zhang, G., He, P., Gaedcke, J., Ghadimi, M.B., Ried, T., Yfantis, H.G., et al. (2013). Macrophage migration inhibitory factor induces epithelial to mesenchymal transition, enhances tumor aggressiveness and predicts clinical outcome in resected pancreatic ductal adenocarcinoma. Int. J. Cancer *132*, 785–794.
32. Kindt, N., Laurent, G., Nonclercq, D., Journé, F., Ghanem, G., Duvillier, H., Gabius, H.J., Lechien, J., and Saussez, S. (2013). Pharmacological inhibition of macrophage migration inhibitory factor interferes with the proliferation and invasiveness of squamous carcinoma cells. Int. J. Oncol. *43*, 185–193.
33. Subbannayya, T., Leal-Rojas, P., Barbhuiya, M.A., Raja, R., Renuse, S., Sathe, G., Pinto, S.M., Syed, N., Nanjappa, V., Patil, A.H., et al. (2015). Macrophage migration inhibitory factor - a therapeutic target in gallbladder cancer. BMC Cancer *15*, 843.
34. Leelawat, K., Narong, S., Udomchaiprasertkul, W., Leelawat, S., and Tungpradubkul, S. (2009). Inhibition of PI3K increases oxaliplatin sensitivity in cholangiocarcinoma cells. Cancer Cell Int. *9*, 3.
35. Yothaisong, S., Dokduang, H., Techasen, A., Namwat, N., Yongvanit, P., Bhudhisawasdi, V., Puapairoj, A., Riggins, G.J., and Loilome, W. (2013). Increased activation of PI3K/AKT signaling pathway is associated with cholangiocarcinoma metastasis and PI3K/mTOR inhibition presents a possible therapeutic strategy. Tumour Biol. *34*, 3637–3648.
36. Jankauskas, S.S., Wong, D.W.L., Bucala, R., Djudjaj, S., and Boor, P. (2019). Evolving complexity of MIF signaling. Cell. Signal. *57*, 76–88.
37. Shu, Y.J., Weng, H., Ye, Y.Y., Hu, Y.P., Bao, R.F., Cao, Y., Wang, X.A., Zhang, F., Xiang, S.S., Li, H.F., et al. (2015). SPOCK1 as a potential cancer prognostic marker promotes the proliferation and metastasis of gallbladder cancer cells by activating the PI3K/AKT pathway. Mol. Cancer *14*, 12.
38. Li, Q., and Yang, Z. (2009). Expression of phospho-ERK1/2 and PI3-K in benign and malignant gallbladder lesions and its clinical and pathological correlations. J. Exp. Clin. Cancer Res. *28*, 65.
39. Chung, J.Y., Hong, S.M., Choi, B.Y., Cho, H., Yu, E., and Hewitt, S.M. (2009). The expression of phospho-AKT, phospho-mTOR, and PTEN in extrahepatic cholangiocarcinoma. Clin. Cancer Res. *15*, 660–667.
40. Tan, E.S., Cao, B., Kim, J., Al-Toubah, T.E., Mehta, R., Centeno, B.A., and Kim, R.D. (2021). Phase 2 study of copanlisib in combination with gemcitabine and cisplatin in advanced biliary tract cancers. Cancer *127*, 1293–1300.
41. Musgrove, E.A., Caldon, C.E., Barraclough, J., Stone, A., and Sutherland, R.L. (2011). Cyclin D as a therapeutic target in cancer. Nat. Rev. Cancer *11*, 558–572.
42. Ouyang, W., Luo, W., Zhang, D., Jian, J., Ma, Q., Li, J., Shi, X., Chen, J., Gao, J., and Huang, C. (2008). PI-3K/Akt pathway-dependent cyclin D1 expression is responsible for arsenite-induced human keratinocyte transformation. Environ. Health Perspect. *116*, 1–6.
43. Shimura, T., Noma, N., Oikawa, T., Ochiai, Y., Kakuda, S., Kuwahara, Y., Takai, Y., Takahashi, A., and Fukumoto, M. (2012). Activation of the AKT/cyclin D1/Cdk4 survival signaling pathway in radioresistant cancer stem cells. Oncogenesis *1*, e12.
44. Bakin, A.V., Tomlinson, A.K., Bhowmick, N.A., Moses, H.L., and Arteaga, C.L. (2000). Phosphatidylinositol 3-kinase function is required for transforming growth factor beta-mediated epithelial to mesenchymal transition and cell migration. J. Biol. Chem. *275*, 36803–36810.
45. Shibue, T., and Weinberg, R.A. (2017). EMT, CSCs, and drug resistance: the mechanistic link and clinical implications. Nat. Rev. Clin. Oncol. *14*, 611–629.
46. Dubrovska, A., Kim, S., Salamone, R.J., Walker, J.R., Maira, S.M., García-Echeverría, C., Schultz, P.G., and Reddy, V.A. (2009). The role of PTEN/Akt/PI3K signaling in the maintenance and viability of prostate cancer stem-like cell populations. Proc. Natl. Acad. Sci. USA *106*, 268–273.

47. Tao, L., Shu-Ling, W., Jing-Bo, H., Ying, Z., Rong, H., Xiang-Qun, L., Wen-Jie, C., and Lin-Fu, Z. (2020). MiR-451a attenuates doxorubicin resistance in lung cancer via suppressing epithelialmesenchymal transition (EMT) through targeting c-Myc. Biomed. Pharmacother. *125*, 109962.

48. Sun, W., Li, J., Zhou, L., Han, J., Liu, R., Zhang, H., Ning, T., Gao, Z., Liu, B., Chen, X., and Ba, Y. (2020). The c-Myc/miR-27b-3p/ATG10 regulatory axis regulates chemoresistance in colorectal cancer. Theranostics *10*, 1981–1996.

49. Moustakas, A., and Heldin, C.H. (2007). Signaling networks guiding epithelial-mesenchymal transitions during embryogenesis and cancer progression. Cancer Sci. *98*, 1512–1520.

50. Vermeulen, L., De Sousa E Melo, F., van der Heijden, M., Cameron, K., de Jong, J.H., Borovski, T., Tuynman, J.B., Todaro, M., Merz, C., Rodermond, H., et al. (2010). Wnt activity defines colon cancer stem cells and is regulated by the microenvironment. Nat. Cell Biol. *12*, 468–476.

51. Espinoza, I., and Miele, L. (2013). Deadly crosstalk: Notch signaling at the intersection of EMT and cancer stem cells. Cancer Lett. *341*, 41–45.

52. Gonzalez, D.M., and Medici, D. (2014). Signaling mechanisms of the epithelial-mesenchymal transition. Sci. Signal. *7*, re8.

53. Stine, Z.E., Walton, Z.E., Altman, B.J., Hsieh, A.L., and Dang, C.V. (2015). MYC, Metabolism, and Cancer. Cancer Discov. *5*, 1024–1039.

54. Chen, D., Huang, J., Zhang, K., Pan, B., Chen, J., De, W., Wang, R., and Chen, L. (2014). MicroRNA-451 induces epithelial-mesenchymal transition in docetaxel-resistant lung adenocarcinoma cells by targeting proto-oncogene c-Myc. Eur. J. Cancer *50*, 3050–3067.

55. Hong, K.O., Kim, J.H., Hong, J.S., Yoon, H.J., Lee, J.I., Hong, S.P., and Hong, S.D. (2009). Inhibition of Akt activity induces the mesenchymal-to-epithelial reverting transition with restoring E-cadherin expression in KB and KOSCC-25B oral squamous cell carcinoma cells. J. Exp. Clin. Cancer Res. *28*, 28.

56. Bian, H.B., Pan, X., Yang, J.S., Wang, Z.X., and De, W. (2011). Upregulation of microRNA-451 increases cisplatin sensitivity of non-small cell lung cancer cell line (A549). J. Exp. Clin. Cancer Res. *30*, 20.

57. van Zandwijk, N., Pavlakis, N., Kao, S.C., Linton, A., Boyer, M.J., Clarke, S., Huynh, Y., Chrzanowska, A., Fulham, M.J., Bailey, D.L., et al. (2017). Safety and activity of microRNA-loaded minicells in patients with recurrent malignant pleural mesothelioma: a first-in-man, phase 1, open-label, dose-escalation study. Lancet Oncol. *18*, 1386–1396.

58. Hong, D.S., Kang, Y.K., Borad, M., Sachdev, J., Ejadi, S., Lim, H.Y., Brenner, A.J., Park, K., Lee, J.L., Kim, T.Y., et al. (2020). Phase 1 study of MRX34, a liposomal miR-34a mimic, in patients with advanced solid tumours. Br. J. Cancer *122*, 1630–1637.

59. Chakraborty, C., Sharma, A.R., Sharma, G., and Lee, S.S. (2021). Therapeutic advances of miRNAs: A preclinical and clinical update. J. Adv. Res. *28*, 127–138.

60. Li, W.J., Wang, Y., Liu, R., Kasinski, A.L., Shen, H., Slack, F.J., and Tang, D.G. (2021). MicroRNA-34a: Potent Tumor Suppressor, Cancer Stem Cell Inhibitor, and Potential Anticancer Therapeutic. Front. Cell Dev. Biol. *9*, 640587.

61. Orellana, E.A., Tenneti, S., Rangasamy, L., Lyle, L.T., Low, P.S., and Kasinski, A.L. (2017). FolamiRs: Ligand-targeted, vehicle-free delivery of microRNAs for the treatment of cancer. Sci. Transl. Med. *9*, eaam9327.

62. Zanoni, M., Piccinini, F., Arienti, C., Zamagni, A., Santi, S., Polico, R., Bevilacqua, A., and Tesei, A. (2016). 3D tumor spheroid models for *in vitro* therapeutic screening: a systematic approach to enhance the biological relevance of data obtained. Sci. Rep. *6*, 19103.

63. Weiswald, L.B., Bellet, D., and Dangles-Marie, V. (2015). Spherical cancer models in tumor biology. Neoplasia *17*, 1–15.

64. Friedrich, J., Seidel, C., Ebner, R., and Kunz-Schughart, L.A. (2009). Spheroid-based drug screen: considerations and practical approach. Nat. Protoc. *4*, 309–324.

65. Patrick, D.M., Zhang, C.C., Tao, Y., Yao, H., Qi, X., Schwartz, R.J., Jun-Shen Huang, L., and Olson, E.N. (2010). Defective erythroid differentiation in miR-451 mutant mice mediated by 14-3-3zeta. Genes Dev. *24*, 1614–1619.

66. Nakano, Y., Tanno, S., Koizumi, K., Nishikawa, T., Nakamura, K., Minoguchi, M., Izawa, T., Mizukami, Y., Okumura, T., and Kohgo, Y. (2007). Gemcitabine chemoresistance and molecular markers associated with gemcitabine transport and metabolism in human pancreatic cancer cells. Br. J. Cancer *96*, 457–463.

67. Ochiai, M., Yoshihara, Y., Maru, Y., Matsuura, T., Izumiya, M., Imai, T., and Hippo, Y. (2019). Kras-driven heterotopic tumor development from hepatobiliary organoids. Carcinogenesis. https://doi.org/10.1093/carcin/bgz024.

68. Chen, W., Wong, C., Vosburgh, E., Levine, A.J., Foran, D.J., and Xu, E.Y. (2014). High-throughput image analysis of tumor spheroids: a user-friendly software application to measure the size of spheroids automatically and accurately. J. Vis. Exp. *89*, 51639.

69. Crowley, L.C., Marfell, B.J., and Waterhouse, N.J. (2016). Analyzing Cell Death by Nuclear Staining with Hoechst 33342. Cold Spring Harb. Protoc. *2016*. pdb.prot087205.

70. Livak, K.J., and Schmittgen, T.D. (2001). Analysis of relative gene expression data using real-time quantitative PCR and the 2(-Delta Delta C(T)) Method. Methods *25*, 402–408.

71. Chen, Y., and Wang, X. (2020). miRDB: an online database for prediction of functional microRNA targets. Nucleic Acids Res. *48*, D127–D131.

72. Kehl, T., Kern, F., Backes, C., Fehlmann, T., Stöckel, D., Meese, E., Lenhof, H.P., and Keller, A. (2020). miRPathDB 2.0: a novel release of the miRNA Pathway Dictionary Database. Nucleic Acids Res. *48*, D142–D147.